

Optimal Control of the F_1 -ATPase Molecular Motor

Deepak Gupta,^{†,¶} Steven J. Large,^{†,§} Shoichi Toyabe,[‡] and David A. Sivak^{*,†}

[†]*Department of Physics, Simon Fraser University, Burnaby, British Columbia V5A 1S6, Canada*

[‡]*Department of Applied Physics, Tohoku University, Aoba 6-6-05, Sendai, 980-8579, Japan*

[¶]*Institute for Theoretical Physics, Technical University of Berlin, Hardenbergstr. 36, D-10623 Berlin, Germany*

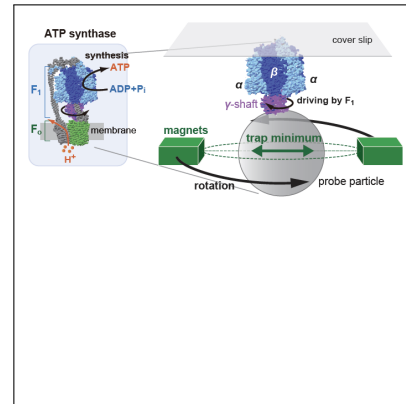
[§]*Current address: Viewpoint Investment Partners, Calgary, Alberta, Canada*

E-mail: dsivak@sfu.ca

Abstract

F_1 -ATPase is a rotary molecular motor that *in vivo* is subject to strong nonequilibrium driving forces. There is great interest in understanding the operational principles governing its high efficiency of free-energy transduction. Here we use a near-equilibrium framework to design a non-trivial control protocol to minimize dissipation in rotating F_1 to synthesize ATP. We find that the designed protocol requires much less work than a naive (constant-velocity) protocol across a wide range of protocol durations. Our analysis points to a possible mechanism for energetically efficient driving of F_1 *in vivo* and provides insight into free-energy transduction for a broader class of biomolecular and synthetic machines.

Graphical TOC Entry



Keywords

molecular motors, stochastic fluctuations, nonequilibrium thermodynamics, free-energy transduction, ATP synthase

Nanometer-sized biomolecular machines convert between different forms of free energy, while remaining in contact with a thermal environment. Consequently, fluctuations play a crucial role in a machine’s dynamics;^{1,2} nevertheless, a machine achieves (on average) directed motion that is consistent with the second law of thermodynamics by transducing free energy, often stored in nonequilibrium chemical concentrations in the surrounding environment.³ It is of paramount interest to unravel the design principles governing effective free-energy transduction in biomolecular machines.^{4–6}

F_oF_1 -ATP synthase has attracted particular attention.^{7–10} This molecular motor is responsible for $\sim 95\%$ of the cellular synthesis of adenosine triphosphate (ATP).^{11,12} ATP production by the F_1 subunit is driven by rotation of its γ -shaft. *In vivo*, the γ -shaft rotates by utilizing free energy from proton flux through the membrane-embedded F_o subunit. The γ -shaft can rotate as fast as ~ 350 revolutions per second,⁹ while maintaining high efficiency.¹³ It is thus of significant interest to measure and quantitatively understand energy conversion during rapid mechanical driving of F_1 to synthesize ATP.^{14–16}

F_oF_1 can operate in either direction:¹⁷ An excess of ATP drives counter-rotation of the γ -shaft and transports protons against their concentration difference. This reversibility is also observed in isolated F_1 , which under sufficiently high torque synthesizes ATP,^{18,19} but in the absence of torque hydrolyzes ATP and counter-rotates the γ -shaft.^{17,20} Experiments suggest that this ‘hydrolysis mode’ proceeds via 120° rotations of the γ -shaft,²¹ composed of two sub-steps: an 80° step involving ATP binding, and a 40° step involving ATP hydrolysis (catalysis).²² Overall the γ -shaft rotates 360° by hydrolyzing 3 ATPs.

Rapidly driving the γ -shaft by applying external torque inevitably produces dissipation, the difference between the work performed and the free energy transduced during synthesis or hydrolysis. It remains enigmatic how ATP synthase achieves highly efficient energetic conversion despite such rapid operation. In particular, what manner of rapid forced rotation with the

γ -shaft achieves efficient energy transmission?

Here we theoretically address efficient driving procedures (*protocols*) to rapidly force rotation of the γ -shaft. A near-equilibrium framework²³ has proven experimentally useful in designing a protocol for switching between folded and unfolded conformations of single DNA hairpins,²⁴ and similarly successful in simulations of barrier crossing,^{25,26} rotary motors,²⁷ Ising models,^{28–30} and other model systems.^{31–34} In this Letter we design a protocol that (near equilibrium) minimizes dissipation in experimentally accessible rotation of the γ -shaft driving F_1 to synthesize ATP. We find that the designed protocol outperforms the naive (constant-velocity) protocol for a considerable range of protocol durations, often far from equilibrium. Such protocols hint at how F_o might rotate the γ -shaft in an efficient manner.

The totally asymmetric allosteric model (TASAM)³⁵ of F_1 describes the evolution of a rotational degree of freedom $\theta \in [0, 2\pi]$ obeying periodic boundary conditions, corresponding to a bead attached to the γ -shaft (Fig. 1a provides a schematic of the modeled experiment). The TASAM is constructed to recover the steady-state and kinetic behavior of F_1 hydrolyzing ATP during single-molecule experiments.^{36,37} The $\ell = 40^\circ$ step is modeled by the system switching between two harmonic potentials of the same spring constant $k \approx 20 k_B T / \text{rad}^2$, and with minima offset by the free-energy difference $\widetilde{\Delta\mu} = 5.2 k_B T$ between the catalytic-dwell and binding-dwell states. Coarse-graining over the fast 40° step gives the effective potential

$$\beta U_n(\theta) \equiv -\ln \left[e^{-\frac{1}{2}\beta k(\theta+\ell-n\xi)^2 - \beta \widetilde{\Delta\mu}} + e^{-\frac{1}{2}\beta k(\theta-n\xi)^2} \right], \quad (1)$$

for $n = 0, \pm 1, \pm 2, \dots$. $\beta \equiv 1/(k_B T)$ is the inverse temperature. The first and second terms in square brackets respectively indicate the catalytic-dwell and binding-dwell states. The 80° step is modeled by a hop between adjacent effective potentials $U_n(\theta)$ and $U_{n\pm 1}(\theta)$ angularly separated by $\xi = 2\pi/3$ rad [see $U_{1,2}(\theta)$ in Fig. 1b].

Thus, the overall hydrolysis/synthesis of one ATP molecule is modeled by switching the ef-

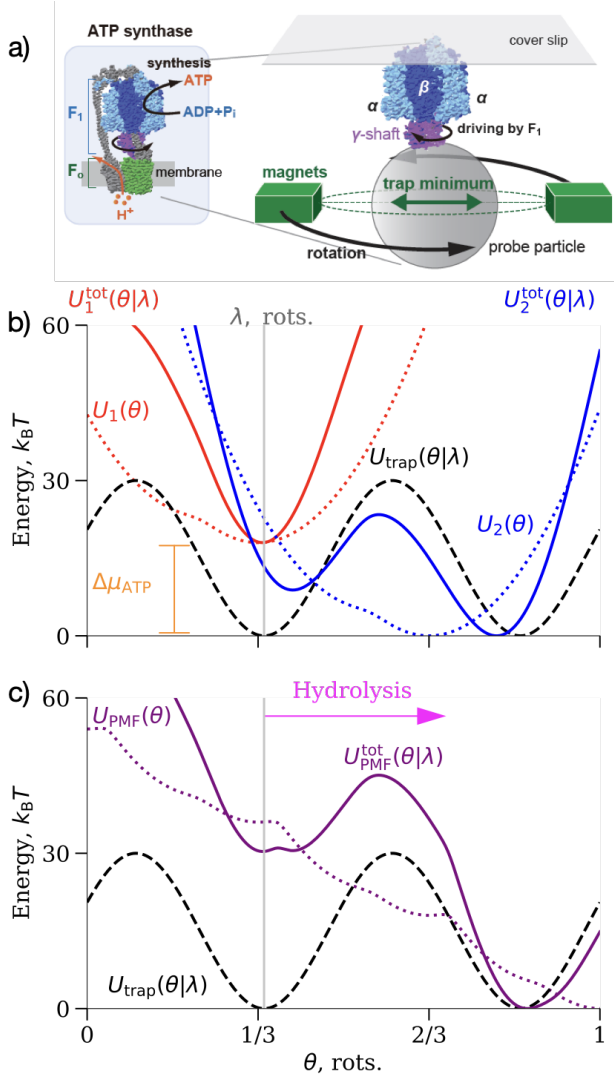


Figure 1: a) Schematic of modeled experiment. b) Effective potential $U_{1,2}(\theta)$ (dotted), trap potential $U_{\text{trap}}(\theta|\lambda)$ (black dashed), and total potentials $U_{1,2}^{\text{tot}}(\theta|\lambda) \equiv U_{1,2}(\theta) + U_{\text{trap}}(\theta|\lambda)$ (solid). c) Potential of mean force $U_{\text{PMF}}(\theta)$ (dotted), trap potential $U_{\text{trap}}(\theta|\lambda)$ (black dashed), and total potential $U_{\text{PMF}}^{\text{tot}}(\theta|\lambda) \equiv U_{\text{PMF}}(\theta) + U_{\text{trap}}(\theta|\lambda)$ (solid). Each potential is plotted as a function of γ -shaft angle θ , for fixed trap minimum $\lambda = 0.41$ (vertical line), chemical drive $\Delta\mu_{\text{ATP}} = 18 k_{\text{B}}T$, and trap strength $E^{\ddagger} = 30 k_{\text{B}}T/\text{rad}^2$.

effective potential, $U_n(\theta) \rightarrow U_{n\pm 1}(\theta)$, where the ‘+’ (‘-’) sign is for hydrolysis (synthesis). The corresponding transition rates obey the local

detailed-balance condition³⁵

$$\frac{R_n^+(\theta)}{R_{n+1}^-(\theta)} = e^{\beta[U_n(\theta) - U_{n+1}(\theta) + \Delta\mu_{\text{ATP}}]} , \quad (2)$$

for chemical-potential difference (hereafter *chemical drive*) $\Delta\mu_{\text{ATP}} \geq 0$ due to synthesis of one ATP, favoring ATP hydrolysis and γ -shaft counter-rotation. The potential switches with respective forward and backward transition rates

$$R_n^+(\theta) = \Gamma, \quad (3a)$$

$$R_{n+1}^-(\theta) = \Gamma e^{-\beta[U_n(\theta) - U_{n+1}(\theta) + \Delta\mu_{\text{ATP}}]} . \quad (3b)$$

Γ is a rate constant characterizing the chemical reaction (Supporting Information³⁸ and Fig. S1 relate Γ and $[\text{ATP}]$ at fixed $\Delta\mu_{\text{ATP}}$). Among the range of possible splittings of angular dependence between the forward and backward transition rates that satisfy local detailed-balance (2), the experimental kinetics in Refs.^{36,37} are best fit by this splitting.³⁵

Experimentally, F_1 is driven by confining the magnetic bead attached to the γ -shaft in a magnetic trap,^{18,19,39,40} whose minimum is dynamically rotated. Modeling such a magnetic trap, here we consider a sinusoidal trap potential (see Fig. 1),

$$U_{\text{trap}}(\theta|\lambda) \equiv -\frac{1}{2}E^{\ddagger} \cos 2(\theta - 2\pi\lambda) , \quad (4)$$

with time-dependent control parameter $\lambda \in [0, 1]$ determining the angle of the two minima differing by 180° and separated by barriers of height E^{\ddagger} (parametrizing trap strength).

Thus, subject to this external trap, the γ -shaft angle θ dynamically evolves according to

$$\dot{\theta} = -\beta D \partial_\theta U_n^{\text{tot}}(\theta|\lambda) + \sqrt{2D} \eta(t) , \quad (5)$$

where the dot indicates a time derivative, $U_n^{\text{tot}}(\theta|\lambda) \equiv U_n(\theta) + U_{\text{trap}}(\theta|\lambda)$ is the total potential, $D = 13.7 \text{ rad}^2/\text{s}$ is the rotational diffusion constant,³⁶ and $\eta(t)$ is Gaussian white noise with zero mean and unit variance. For $\Delta\mu_{\text{ATP}} \neq 0$, the system eventually reaches a nonequilibrium steady state.⁴¹ Chemical transition rates (3) and mechanical dynamics (5), subject to potentials (1) and (4), constitute the

TASAM.

In the limit of fast switching between effective potentials when chemistry is fast compared to mechanics ($\Gamma \rightarrow \infty$, e.g., at high [ATP]),³⁵ the dynamics (5) reduce to

$$\dot{\theta} = -\beta D \partial_{\theta} U_{\text{PMF}}^{\text{tot}}(\theta|\lambda) + \sqrt{2D} \eta(t), \quad (6)$$

for total potential energy $U_{\text{PMF}}^{\text{tot}}(\theta|\lambda) \equiv U_{\text{PMF}}(\theta) + U_{\text{trap}}(\theta|\lambda)$ and potential of mean force, averaging over all effective potentials (see Fig. 1c):

$$\beta U_{\text{PMF}}(\theta) \equiv -\ln \sum_{n=-\infty}^{+\infty} e^{-\beta[U_n(\theta) - n\Delta\mu_{\text{ATP}}]}. \quad (7)$$

We seek a driving protocol that minimizes dissipation while rotating the γ -shaft (for theoretical developments when control is much finer-grained, see Refs.^{42,43}). For a harmonically confined Brownian particle, minimum-dissipation protocols have been analytically solved for arbitrary protocol duration.^{44,45} For more complicated scenarios such as this model, no analytical solution is known; nevertheless, linear-response theory gives an approximately dissipation-minimizing protocol.²³ Up to the linear-response approximation, the instantaneous excess power (that exceeding the quasistatic power) during dynamic variation of control parameter λ is

$$P_{\text{ex}}(t) \approx \zeta(\lambda) \left(\frac{d\lambda}{dt} \right)^2. \quad (8)$$

Its time integral over protocol duration t_{prot} gives the excess work $W_{\text{ex}} \equiv W - \Delta F = \int_0^{t_{\text{prot}}} dt P_{\text{ex}}(t)$, for protocol work W and equilibrium free-energy change ΔF from initial to final control-parameter values. $\zeta(\lambda)$ is a generalized friction coefficient obtained here by integrating the equilibrium torque autocovariance:

$$\zeta(\lambda) \equiv \beta \int_0^{\infty} dt \langle \delta\tau(0) \delta\tau(t) \rangle_{\lambda}. \quad (9)$$

Angle brackets $\langle \dots \rangle_{\lambda}$ indicate a steady-state average at fixed λ . $\delta\tau(t) \equiv \tau(t) - \langle \tau \rangle_{\lambda}$ is the deviation of the conjugate torque $\tau \equiv -\partial_{\lambda} U_{\text{trap}}(\theta|\lambda) = 2\pi E^{\ddagger} \sin 2(\theta - 2\pi\lambda)$ from its

equilibrium average. The generalized friction coefficient can be decomposed as

$$\zeta(\lambda) = \beta \langle (\delta\tau)^2 \rangle_{\lambda} t_{\text{relax}}(\lambda), \quad (10)$$

the product of the torque variance $\langle (\delta\tau)^2 \rangle_{\lambda}$ and the torque relaxation time

$$t_{\text{relax}}(\lambda) \equiv \int_0^{\infty} dt \frac{\langle \delta\tau(0) \delta\tau(t) \rangle_{\lambda}}{\langle (\delta\tau)^2 \rangle_{\lambda}}. \quad (11)$$

In the linear-response regime, the minimum-dissipation protocol proceeds with velocity inversely proportional to the square root of the generalized friction coefficient:²³

$$\frac{d\lambda^{\text{des}}}{dt} \propto [\zeta(\lambda)]^{-1/2}. \quad (12)$$

Dissipation is reduced by driving slower where system resistance is greatest (due to large fluctuations and/or slow relaxation) and compensating by driving faster where system resistance is least. Imposing boundary conditions $\lambda(0) = \lambda_i$ and $\lambda(t_{\text{prot}}) = \lambda_f$ fixes the proportionality constant. Such a designed protocol $\lambda^{\text{des}}(t)$ gives (up to linear response) constant excess power.

Figure 2a shows $U_{\text{PMF}}^{\text{tot}}(\theta|\lambda)$ for different trap minima λ and fast switching. For some λ 's, the total potential has two metastable states, with a small ($< 0.5 k_{\text{B}}T$) barrier.

The friction coefficient (9) is obtained through measurement of the equilibrium torque autocovariance for a stationary trap (i.e., fixed λ) and hence fixed total potential-energy landscape (Fig. 2a). Figure 2b shows this torque autocovariance function. For those trap minima λ giving two metastable states (Fig. 2a), the torque autocovariance relaxes particularly slowly.

Figure 2c shows the torque variance computed from the equilibrium torque fluctuations. The torque variance is independent of Γ , as expected since varying Γ modifies system relaxation between landscapes but not the landscapes themselves. Similarly, Fig. 2d shows the torque relaxation time (11), $t_{\text{relax}}(\lambda)$. The product of the torque variance and torque relaxation time gives the generalized friction co-

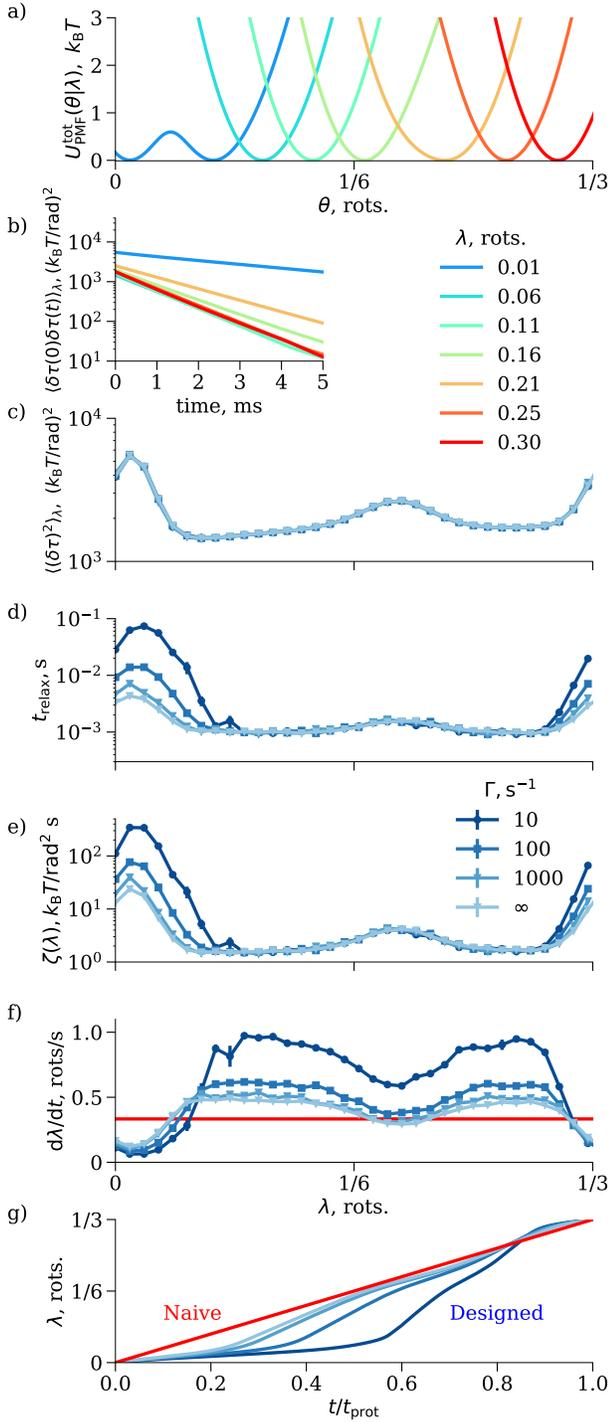


Figure 2: (a) Total potential energy as a function of γ -shaft angle θ . (b) Torque autocovariance as a function of time. (c) Torque variance, (d) torque relaxation time, (e) friction coefficient, and (f) protocol velocity, each as a function of trap minimum λ . (g) Protocol as a function of time. (f,g) Red lines: naive (constant-velocity) protocols; points/curves: designed protocols. Potential switching rate $\Gamma = \infty$ (a,b), and 10/100/1000/ ∞ s^{-1} (c-g). Throughout, trap strength $E^\ddagger = 30 k_B T / \text{rad}^2$ and chemical drive $\Delta\mu_{\text{ATP}} = 18 k_B T$. In all figures, error bars show one standard error of the mean.

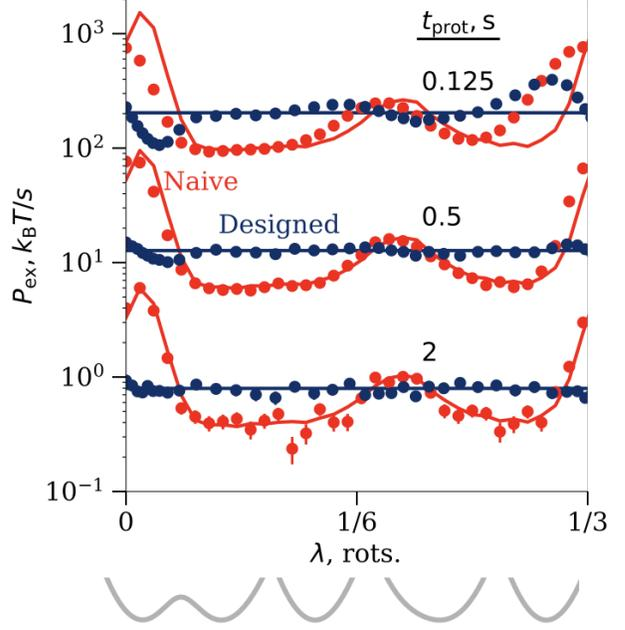


Figure 3: Steady-state excess power while driving ATP synthesis, as a function of trap minimum λ , for protocol durations $t_{\text{prot}} = 0.125, 0.5,$ and 2 s, for naive (red) and designed (blue) protocols (Fig. 2g) in the full model (points) and the linear-response approximation (8) (curves). Throughout, trap strength $E^\ddagger = 30 k_B T / \text{rad}^2$, chemical drive $\Delta\mu_{\text{ATP}} = 18 k_B T$, and potential switching rate $\Gamma \rightarrow \infty$. Gray curves at bottom depict the total potential at the corresponding trap minimum.

efficient (Fig. 2e). The peak relaxation time (generally for trap minimum λ such that the system has significant probability in multiple potentials) is higher for smaller Γ , which slows system relaxation between distinct potentials. The torque variance, torque relaxation time, and friction coefficient each have a local maximum for the trap minimum near the shoulder of $U_n(\theta)$ (Fig. 1b) and $U_{\text{PMF}}(\theta)$ (Fig. 1c). As expected, these local maxima in friction coefficient coincide with the experimental local minima of F_1 's rotational velocity during hydrolysis.¹⁵

According to (12), excess work is reduced by slowing down where friction is high, giving more time for thermal fluctuations to overcome the energy barrier separating metastable states (Fig. 2a) and thereby reducing necessary work.

Figure 2f compares the control-parameter velocities of designed protocols and naive ones (i.e., with constant velocity). Integrating the control-parameter velocity gives the protocol as a function of time (Fig. 2g).

To compute excess power and work, we numerically simulate (without assuming linear response) the full model of the system, Eqs. 5 and 6, driven by naive and designed protocols across a full rotation driving ATP synthesis (decreasing λ).

Figure 3 shows the steady-state excess power of the full model for fast potential switching rate ($\Gamma \rightarrow \infty$), with the linear-response approximation (8) as a reference. The linear-response approximation is quite accurate in the long-duration limit since the system remains sufficiently close to equilibrium. For the naive protocol, excess power is strongly peaked where the γ -shaft experiences high resistance (Fig. 2e). The designed protocol compensates by driving slower there (Fig. 2d), thereby flattening the excess power across the protocol.

Finally, Figure 4a shows excess work during naive and designed protocols driving ATP synthesis, for different switching rates Γ . As expected, the work decreases with protocol duration and with Γ . For longer durations, the linear-response approximation is quite accurate.

Figure 4b shows the ratio of excess work during naive and designed protocols. For the slowest protocols and slowest switching rate, designed protocols reduce excess work $\sim 2.5\times$ compared to naive. At longer protocol duration, the excess-work ratio for the slowest switching rate is almost twice that of the fastest switching rate ($\Gamma \rightarrow \infty$). A slower switching rate produces greater variation in the friction coefficient (Fig. 2e), leading to designed protocols that differ more from naive ones (Fig. 2g) and thus offering greater advantage to using designed protocols.

Analogous driving of ATP hydrolysis (instead of synthesis) and different trap strengths and chemical drives produce qualitatively similar generalized friction coefficients and designed protocols (Fig. S2), excess power along the protocol (Fig. S3), and excess work (Figs. S4 and

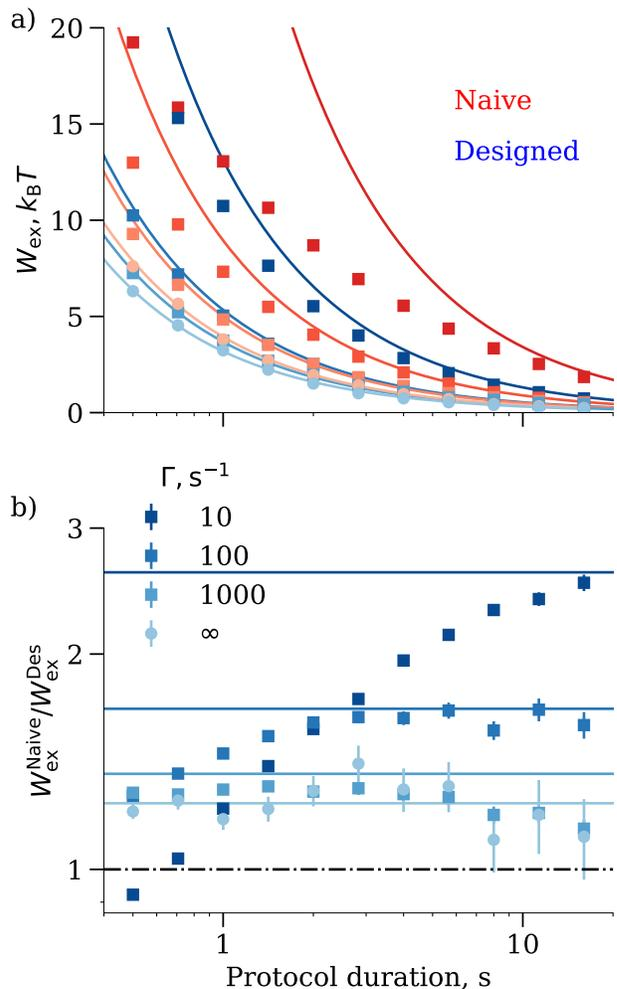


Figure 4: Excess work while driving ATP synthesis. a) Naive (red) and designed (blue) excess works. b) Ratio of naive and designed excess works. Points show the full model and curves the linear-response approximation. Color intensity decreases with switching rate Γ . Throughout, trap strength $E^\ddagger = 30 k_B T/\text{rad}^2$ and chemical drive $\Delta\mu_{\text{ATP}} = 18 k_B T$.

S5).

We have studied nonequilibrium driving of an experimentally motivated model^{35,36} of the F_1 -ATPase molecular motor. We found that the designed protocol (that near equilibrium minimizes work) indeed significantly decreases work for a wide range of protocol durations, including some driving F_1 far from equilibrium and dissipating as much as several $k_B T$ per ATP synthesized. This demonstrates the utility of this linear-response framework significantly beyond its regime of strict validity. This protocol allo-

cates more time to regions where fluctuations are large and/or relaxation is slow (and where F_1 rotates slowest when hydrolyzing ATP¹⁵), and hence where greater time for system relaxation can make the most difference. In this model this is where the total potential is bimodal, due to F_1 fluctuating between distinct chemical states with correspondingly different mechanics.

Recent work has derived optimal protocols in the opposite limit of very fast driving;⁴⁶ these rapid protocols, and interpolations between them and near-equilibrium ones, would allow systematic characterization of efficiency across driving speeds. Our simple near-equilibrium theory may also be helpful in physically constraining machine-learning algorithms⁴⁷ or in more direct numerical calculation⁴⁸ of optimal protocols far from equilibrium. Moreover, there is promise in exploring near-optimal protocols,⁴⁹ analysis of which significantly broadens the class of successful control strategies.

Our research opens avenues for future experimental investigation with an analogous setup to Refs.^{39,40} Such an experiment can be used to design and implement a rotational driving protocol employing our methodology. Our study predicts experimental conditions where such designs will produce substantial energy savings, informing experiments to either drive F_1 to efficiently produce ATP or efficiently harness mechanical energy from ATP hydrolysis.

The F_oF_1 molecular motor transduces energy at high efficiency.⁵⁰ Our designed protocol may mimic an operational mechanism by which F_o rotates F_1 's γ -shaft to synthesize ATP, driving slower where friction is higher, which we predict would save energy compared to constant-velocity driving. It would be interesting to probe the actual stochastic dynamics by which F_o mechanically drives F_1 *in vivo* and understand its correspondence to an effective nonequilibrium driving protocol. E.g., F_o could approximate such a protocol if its metastable rotational states are out of phase with those of F_1 . More generally, our methodology may be applied to identify design principles for nanoscale free-energy transduction within and between other molecular machines.

Acknowledgement We thank Alex Tong and Carlos Bustamante (Berkeley Physics) for enlightening discussions, and Adrienne Zhong (Berkeley Physics) for feedback on the manuscript. This work was supported by a Natural Sciences and Engineering Research Council of Canada (NSERC) Discovery Grant (D.A.S.), a Tier-II Canada Research Chair (D.A.S.), and the Deutsche Forschungsgemeinschaft (DFG, German Research Foundation) - Projekt-nummer 163436311 - SFB 910 (D.G.), and was enabled in part by support provided by BC DRI Group and the Digital Research Alliance of Canada (www.alliancecan.ca).

Supporting Information Available

Supporting Information contains further numerical simulation results and details of simulation methods.

Supporting Information

Relating Γ to [ATP]

Figure S1a shows experimental rotational rates from:³⁷ The rotation rate strongly increases with [ATP] and weakly increases with $\Delta\mu_{\text{ATP}}$. Figure S1b shows numerical Langevin simulations of the rotation rate as a function of Γ : The rotation rate increases with Γ and asymptotes to the rotation rate for fast-switching dynamics (6) ($\Gamma \rightarrow \infty$). At fixed $\Delta\mu_{\text{ATP}}$, comparing Figs. S1a and b permits calibration of switching rate Γ : Γ ranging from 1 to 1,000 Hz reproduces rotational rates for [ATP] ranging from 0.1 to 100 μM .

Torque fluctuations and designed protocol for $\Gamma \rightarrow \infty$: varying E^\ddagger and $\Delta\mu_{\text{ATP}}$

Figures S2a-d respectively show the torque variance, torque relaxation time, friction coefficient, and rate of change of protocol, each as a function of trap minimum λ , for two trap strengths E^\ddagger and three chemical drives $\Delta\mu_{\text{ATP}}$. Figure S2e shows the naive and designed protocols obtained by integrating their respective protocol velocities (Fig. S2d)

The torque variance empirically increases with trap strength E^\ddagger ; this is intuitive, as in a simple quadratic potential the equipartition theorem⁵¹ dictates that the torque variance is directly proportional to E^\ddagger . The torque variance, torque relaxation time, and friction coefficient each are globally maximized at the trap minimum λ where $U_{\text{PMF}}^{\text{tot}}(\theta|\lambda)$ has two metastable states (see the leftmost potential in Fig. 2a), and have a local maximum for λ at the PMF's shoulder (Fig. 1c). The friction coefficient's maximum value decreases with trap strength E^\ddagger , because the barrier height in the

double-well total potential $U_{\text{PMF}}^{\text{tot}}(\theta|\lambda)$ decreases with E^\ddagger . Further, the global maximum shifts leftwards as $\Delta\mu_{\text{ATP}}$ increases since this reduces the λ at which the total potential $U_{\text{PMF}}^{\text{tot}}$ has two metastable states, and the insensitivity of U_{PMF} 's shoulder to variation of $\Delta\mu_{\text{ATP}}$ reflects that the local maximum is similarly insensitive.

Excess power for $\Gamma \rightarrow \infty$: varying direction, E^\ddagger , and $\Delta\mu_{\text{ATP}}$

Figure S3 compares the steady-state excess power P_{ex} as a function of trap minimum λ , during driven hydrolysis (increasing λ) and synthesis (decreasing λ), for three protocol durations t_{prot} , two trap strengths E^\ddagger , and three chemical drives $\Delta\mu_{\text{ATP}}$. The excess power is qualitatively similar for the two trap strengths, and lower for higher trap strength. Since during hydrolysis the γ -shaft rotates in the opposite manner than during synthesis, the excess power for the full model flips. In contrast, the linear-response approximation is the same for driven synthesis and hydrolysis. For longer durations, the linear-response approximation (8) closely matches the full model, as expected. For intermediate duration, agreement is poor near the peak of the friction coefficient (where linear response predicts that excess power peaks under naive protocols). Agreement is better for a stronger trap since the system mostly follows the trap for the entire duration.

Excess work driving ATP hydrolysis

Figure S4 shows the excess works by rotating the γ -shaft employing the naive and designed

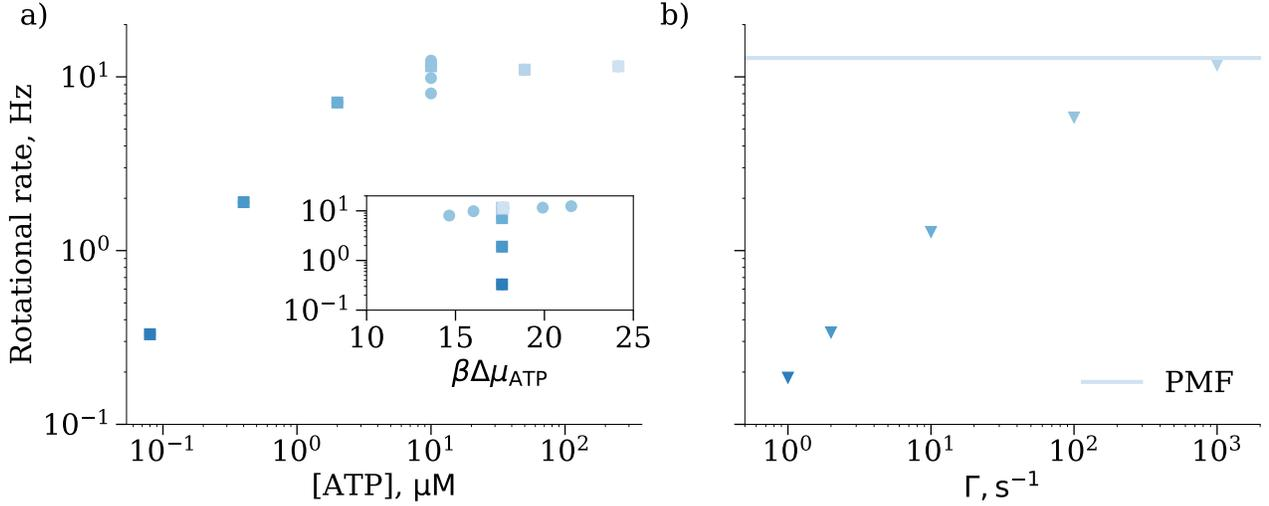


Figure S1: γ -shaft rotation rate (a) in experiment³⁷ as a function of $[\text{ATP}]$ and of chemical drive $\beta\Delta\mu_{\text{ATP}}$ (inset), and (b) in simulation as a function of switching rate Γ for slow-switching dynamics (5) (triangles) or fast-switching dynamics (6) (horizontal line). Color intensity decreases with $[\text{ATP}]$ for chemical drive $\Delta\mu_{\text{ATP}} \approx 17.6 k_{\text{B}}T$.

protocols (see Fig. 2g) to drive ATP hydrolysis, for different values of switching rate Γ . The linear-response approximation is quite accurate in the long-protocol duration limit. Qualitatively, the excess-work features during hydrolysis are similar to those during synthesis, and the ratio of naive to designed excess work for our slowest switching rate ($\Gamma = 10 \text{ s}^{-1}$) is almost double that in the limit $\Gamma \rightarrow \infty$.

Excess work for $\Gamma \rightarrow \infty$: varying direction, E^\ddagger , and $\Delta\mu_{\text{ATP}}$

Figure S5 shows naive and designed excess works and their ratio, $W_{\text{ex}}^{\text{Naive}}/W_{\text{ex}}^{\text{Des}}$,⁵² during driven hydrolysis and synthesis, for two trap strengths and three chemical drives $\Delta\mu_{\text{ATP}}$.

Longer protocol durations keep the system closer to equilibrium, increasing the accuracy of the linear-response approximation. The designed protocol's excess work agrees with its linear-response approximation starting at shorter durations than the naive protocol's does (Fig. S5a).

For virtually all durations explored, designed

protocols save energy compared to naive protocols (Fig. S5b). The performance of designed protocols (relative to naive), as quantified by the ratio of designed to naive excess works, improves with protocol duration until it saturates at the linear-response approximation. This excess-work ratio decreases with trap strength, and is qualitatively similar in both hydrolysis and synthesis directions.

Simulation methods

Torque autocovariance

For $\Gamma \rightarrow \infty$, we discretize the Langevin equation (6) to first order in Δt and compute θ_ℓ ($1 \leq \ell \leq t_{\text{prot}}/\Delta t$) using

$$\theta_\ell = \theta_{\ell-1} + \beta D \tau_{\text{PMF}}^{\text{tot}}(\theta_{\ell-1}|\lambda) \Delta t + \sqrt{2D \Delta t} \tilde{\eta}_{\ell-1}, \quad (\text{S1})$$

where $\tau_{\text{PMF}}^{\text{tot}}(\theta|\lambda) \equiv -\partial_\theta U_{\text{PMF}}^{\text{tot}}(\theta|\lambda)$ is the sum of torques derived from the underlying PMF and trap potential. $\tilde{\eta}_\ell$ is a normal random variable with zero mean and unit variance, and θ_0 is drawn from the canonical distribution, i.e., proportional to $e^{-\beta U_{\text{PMF}}^{\text{tot}}(\theta|\lambda)}$ for $\theta \in [-\pi/2 + 2\pi\lambda, \pi/2 + 2\pi\lambda]$. (Notice that the trap

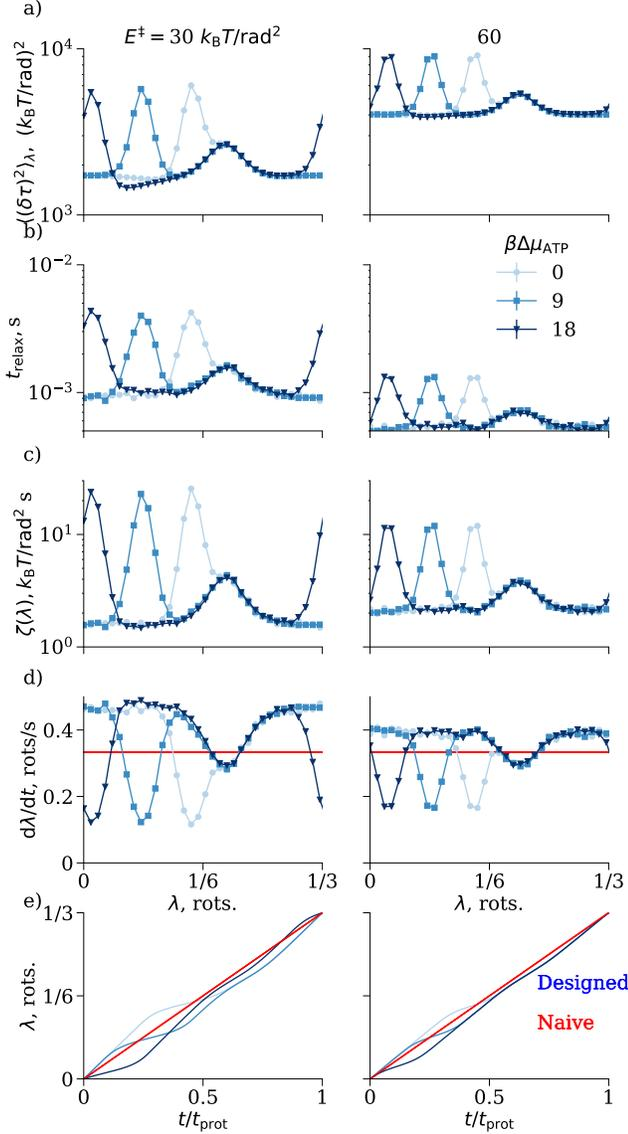


Figure S2: Equilibrium torque fluctuations and designed protocol. (a) Torque variance, (b) torque relaxation time, (c) friction coefficient, and (d) protocol velocity, each as a function of trap minimum, λ . (e) Protocols as a function of time. (d,e) Red lines indicate naive protocols and curves/points indicate designed protocols. Trap strengths $E^\ddagger = 30$ (left) and $60 k_B T / \text{rad}^2$ (right). Color intensity increases with chemical drive $\Delta\mu_{\text{ATP}}$.

potential $U_{\text{trap}}(\theta|\lambda)$ has two minima separated by π rad, and we initialize the γ -shaft's location in the well whose minimum is at $2\pi\lambda$ rad, where $\lambda \in [0, 1]$.) For each fixed trap minimum λ , we generate a time-series of length 500 s of the external torque $\tau_\ell \equiv -\partial_\lambda U_{\text{trap}}(\theta_\ell|\lambda) = 2\pi E^\ddagger \sin 2(\theta_\ell - 2\pi\lambda)$ (see main text). We discard the initial 0.25 s (roughly $50\times$ the torque relaxation time) of each trajectory, and use the remaining part to compute the torque autocovariance function $\langle \delta\tau_0 \delta\tau_\ell \rangle_\lambda$. The torque autocovariance in Fig. 2b is an average over three such trajectories initiated from three different initial conditions θ_0 .

For finite Γ , we again confine the bead attached to the γ -shaft in the sinusoidal potential $U_{\text{trap}}(\theta|\lambda)$ [Eq. (4)], so that the system evolves according to (5) and switches its effective potential U_n following the forward (3a) and backward rates (3b). We follow the same numerical simulation procedure as discussed above for $\Gamma \rightarrow \infty$ to compute the friction coefficient and related quantities displayed in Fig. S2.

Time-integrated average flux

During a protocol, the system in general lags behind the trap's minimum, with magnitude depending on the protocol duration. To quantify rotation of the γ -shaft during a protocol completing a full rotation in a given duration t_{prot} , we numerically compute the time-integrated average flux

$$\bar{J} \equiv \frac{1}{2\pi} \int_0^{t_{\text{prot}}} dt \int_0^{2\pi} d\theta J(\theta, t), \quad (\text{S2})$$

for probability flux $J(\theta, t)$. $\bar{J} = 1$ corresponds to a complete γ -shaft rotation over the course of the respective protocol.

For all observed protocol durations and both protocols, \bar{J} eventually approaches unity (see Sec. "Simulation parameters"), indicating that the system reaches a nonequilibrium steady state.

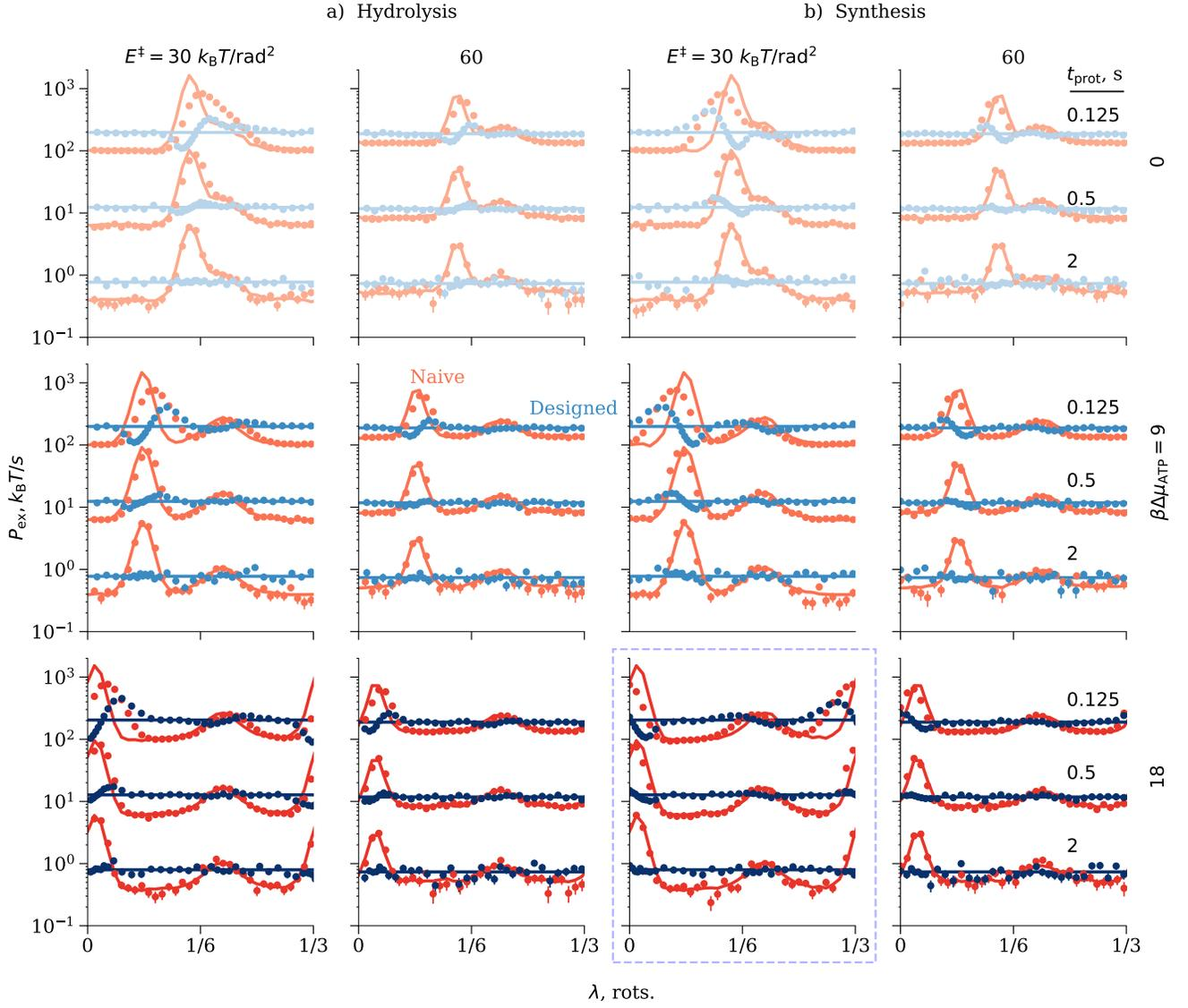


Figure S3: Steady-state excess power as a function of λ , during driven (a) hydrolysis (increasing λ) and (b) synthesis (decreasing λ), naive (red) and designed (blue) protocols, for the full model (points) and the linear-response approximation (8). Blue dashed box indicates data shown in Fig. 3. Trap strengths $E^\ddagger = 30$ and $60 k_B T / \text{rad}^2$, chemical drives $\Delta\mu_{\text{ATP}} = 0, 9$, and $18 k_B T$ (top to bottom), and protocol durations $t_{\text{prot}} = 0.125, 0.5$, and 2 s.

Escape fraction

The external trap has two identical energy wells separated by 180° . When the protocol duration is sufficiently short (so driving is sufficiently rapid), some trajectories cross the intervening barrier to the adjacent well. Our theoretical treatment assumes that the trap is sufficiently strong to prevent any such fluctuation, so we discard these trajectories.

Numerical simulations of the full model show that for $\Gamma \rightarrow \infty$ this escape fraction decreases

(increases) with the chemical drive $\Delta\mu_{\text{ATP}}$ when dynamically driving hydrolysis (synthesis), since the system moves with (against) the potential gradient due to $U_{\text{PMF}}(\theta)$. Similarly, for finite Γ , larger $\Delta\mu_{\text{ATP}}$ favors the γ -shaft's rotation in the hydrolysis direction (3) reducing the proportion of trajectories that escape from the local well.

For $\Gamma \rightarrow \infty$, in the fastest simulated protocols dynamically driving hydrolysis (synthesis) and for the lowest (highest) $\Delta\mu_{\text{ATP}}$, we find

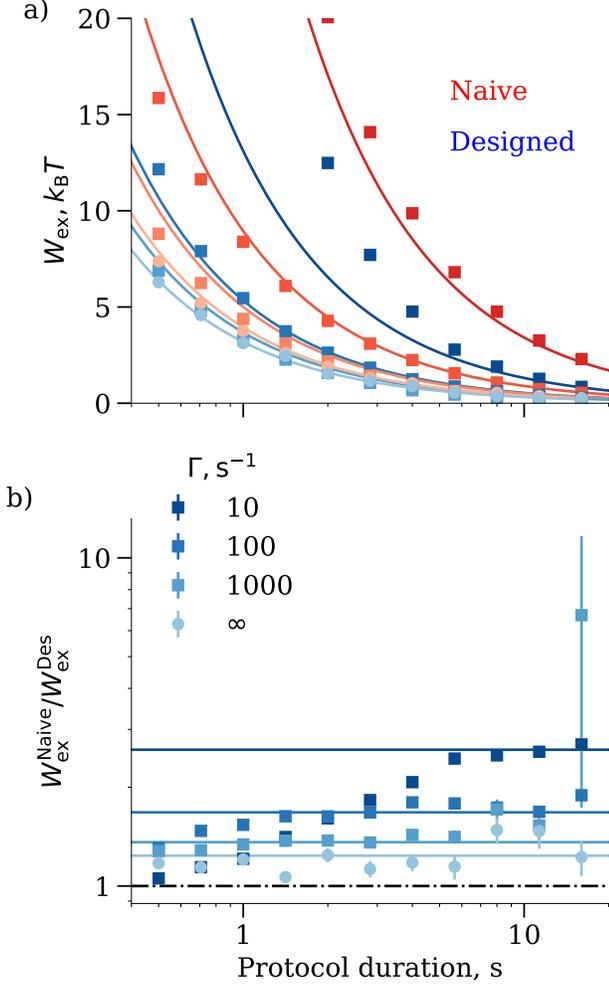


Figure S4: Excess work when driving hydrolysis. (a) Excess work for naive (red) and designed (blue) protocols, and (b) ratio of naive and designed excess works, each as a function of protocol duration, for the full model (points) and the linear-response approximation (curves). Trap strength $E^\ddagger = 30 k_B T / \text{rad}^2$ and chemical drive $\Delta\mu_{\text{ATP}} = 18 k_B T$. Color intensity decreases with switching rate Γ . In all figures, error bars show one standard error of the mean.

that 0.005% (0.5%) of trajectories escape the local trap. The fraction decreases with protocol duration, as expected. For the stronger trap ($E^\ddagger = 60 k_B T / \text{rad}^2$), no trajectories escape across all observed durations.

Excess work

To numerically compute the excess work, we first discretize each protocol for a given protocol duration t_{prot} . We compute the external work during a single trajectory by evaluating the net change in internal energy due to the control-parameter change from an initial value $\lambda_i = 0$ to $\lambda_f = 1$ in t_{prot} :

$$w = \sum_{\ell=0}^{t_{\text{prot}}/\Delta t - 1} [U_{\text{trap}}(\theta_\ell, \lambda_{\ell+1}) - U_{\text{trap}}(\theta_\ell, \lambda_\ell)] , \quad (\text{S3})$$

where θ_ℓ is obtained from the discretized version of the Langevin equation at fixed λ_ℓ , (S1) for $\Gamma \rightarrow \infty$ and analogously for finite Γ . When driving hydrolysis, we advance λ from λ_i to λ_f , whereas when driving synthesis, we reduce it from λ_f to λ_i . The excess work is the work minus the equilibrium free-energy difference: $w_{\text{ex}} \equiv w - \Delta F$. Here $\Delta F = \mp 3\Delta\mu_{\text{ATP}}$, where the ‘-’ (‘+’) sign corresponds to hydrolysis (synthesis), and the factor of 3 represents the 3 ATP hydrolyzed or synthesized per complete rotation. Finally, we average over the \mathcal{N}_R realizations that stay in the trap’s local well (see ‘Escape fraction’ section) to get the excess work $W_{\text{ex}} \equiv \langle w_{\text{ex}} \rangle$. To exclude transient relaxation to the nonequilibrium steady state, we compute the excess work starting after two full rotations (Figs. 4 and S4) or four full rotations (Fig. S5). Similar to the procedure in this section for excess work, we compute time-integrated average flux, escape fraction, and excess power in the numerical simulations.

Simulation parameters

In our model, the system relaxation time in the trap is (to a harmonic approximation) $t_{\text{trap}} \equiv \frac{k_B T}{DE^\ddagger} = 1.2 - 2.4 \times 10^{-3}$ s for trap strengths

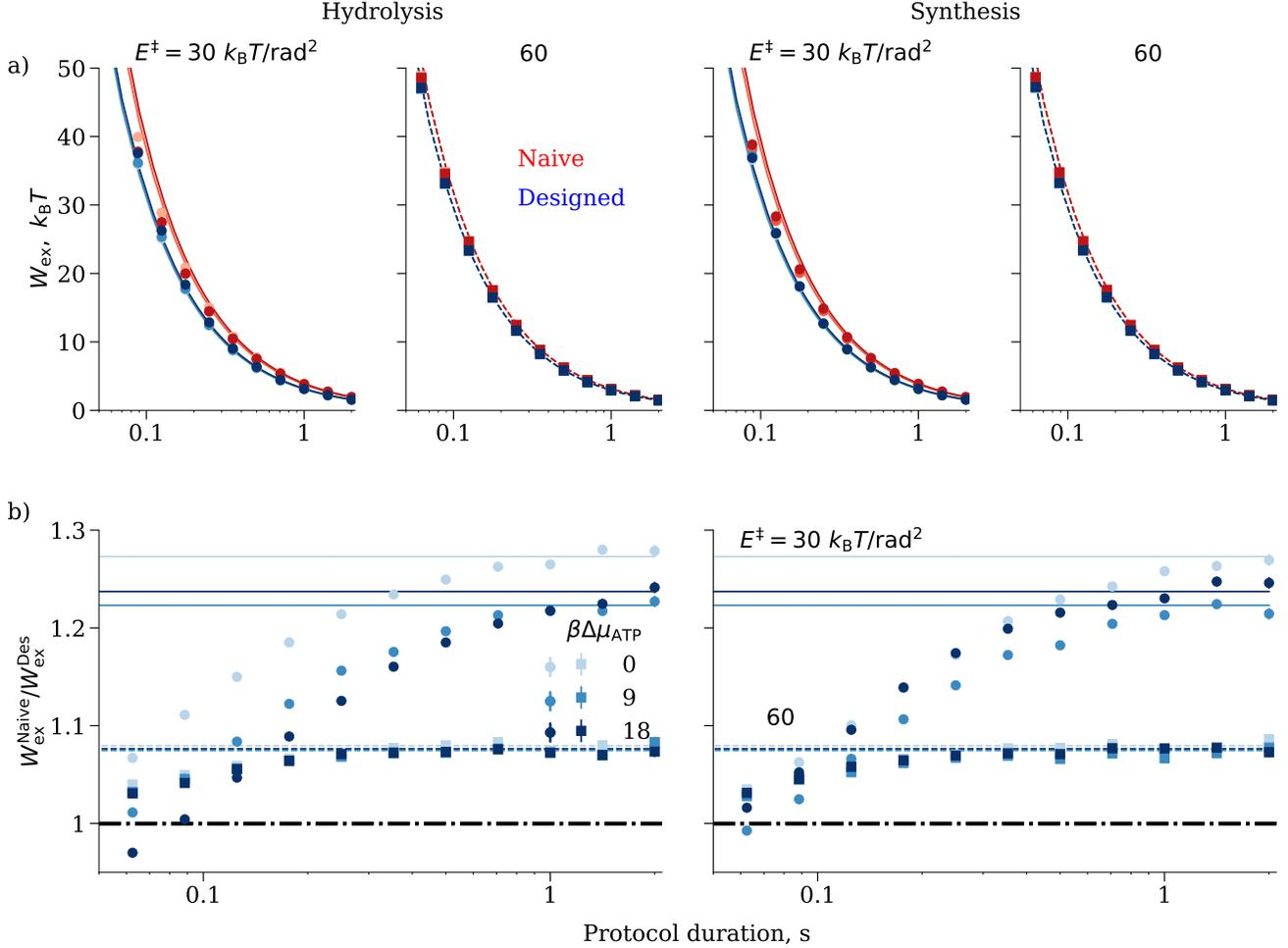


Figure S5: Excess work. (a) Excess work for naive (red) and designed (blue) protocols, and (b) ratio of naive and designed excess works, all as a function of protocol duration t_{prot} , for driven hydrolysis (left) and synthesis (right), for the full model (points) and the linear-response approximation (curves), for trap strengths $E^\ddagger = 30 k_B T / \text{rad}^2$ (circles, solid curves) and $60 k_B T / \text{rad}^2$ (squares, dashed curves). Color intensity increases with the chemical drive $\Delta \mu_{\text{ATP}}$.

$E^\ddagger = 30 k_B T / \text{rad}^2$ and $60 k_B T / \text{rad}^2$, and diffusion constant $D = 13.7 \text{ rad}^2 / \text{s}$. Therefore, for each numerical simulation we generally choose discretization timestep $\Delta t = 10^{-5} \text{ s}$, at least two orders of magnitude shorter than the relaxation time. We average over 3 independent trajectories to obtain the friction coefficient and related observables in Figs. 2(b-g) and S2.

For computing excess work, time-integrated average flux, and escape fraction when $\Gamma \rightarrow \infty$, we rotate the γ -shaft with protocol durations as fast as $t_{\text{prot}} = 2^{-4} \text{ s}$ (i.e., 62.5 ms), $\approx 12.5 \times$ slower than the maximum torque relaxation time ($\sim 5 \text{ ms}$). The data shown in Figs. 3, S3, and S5 are obtained by averaging over 10^5 trajectories during a complete rotation of the γ -

shaft following four complete rotations to allow the system to reach steady state.

For the computation of excess work for finite Γ (Figs. 4 and S4), we rotate the γ -shaft in the range of protocol durations $2^{-1} - 2^4 \text{ s}$, where the fastest protocol has duration $\approx 5 \times$ the maximum of the torque relaxation time for the slowest potential-switching rate ($\Gamma = 10 \text{ s}^{-1}$). We average over 10^3 trajectories during a complete rotation of the γ -shaft following two complete rotations to allow the system to reach steady state. In order to increase the accuracy of the Langevin simulations, we used the discretization time $\Delta t = 10^{-6} \text{ s}$.

For the largest finite Γ and longest protocol durations, this timestep still produces dis-

cretization artifacts (seen in the modest disagreement between the full model and the linear-response approximation in Figs. 4 and S4), but an even shorter timestep is computationally prohibitive.

References

- (1) Seifert, U. Stochastic thermodynamics, fluctuation theorems and molecular machines. *Reports on Progress in Physics* **2012**, *75*, 126001.
- (2) Astumian, R. D.; Bier, M. Fluctuation driven ratchets: Molecular motors. *Phys. Rev. Lett.* **1994**, *72*, 1766–1769.
- (3) Machta, B. B. Dissipation Bound for Thermodynamic Control. *Phys. Rev. Lett.* **2015**, *115*, 260603.
- (4) Mugnai, M. L.; Hyeon, C.; Hinczewski, M.; Thirumalai, D. Theoretical perspectives on biological machines. *Rev. Mod. Phys.* **2020**, *92*, 025001.
- (5) Brown, A. I.; Sivak, D. A. Theory of Nonequilibrium Free Energy Transduction by Molecular Machines. *Chemical Reviews* **2020**, *120*, 434–459.
- (6) Kolomeisky, A. B. Motor proteins and molecular motors: how to operate machines at the nanoscale. *Journal of Physics: Condensed Matter* **2013**, *25*, 463101.
- (7) Boyer, P. D. The binding change mechanism for ATP synthase—some probabilities and possibilities. *Biochimica et Biophysica Acta (BBA)-Bioenergetics* **1993**, *1140*, 215–250.
- (8) Boyer, P. D. The ATP Synthase—A splendid molecular machine. *Annual Review of Biochemistry* **1997**, *66*, 717–749.
- (9) Ueno, H.; Suzuki, T.; Kinosita, K.; Yoshida, M. ATP-driven stepwise rotation of FoF1-ATP synthase. *Proceedings of the National Academy of Sciences* **2005**, *102*, 1333–1338.
- (10) Huxley, A. F.; Simmons, R. M.; Oster, G.; Wang, H.; Grabe, M. How F_o-ATPase generates rotary torque. *Philosophical Transactions of the Royal Society of London. Series B: Biological Sciences* **2000**, *355*, 523–528.
- (11) Yoshida, M.; Muneyuki, E.; Hisabori, T. ATP synthase—a marvellous rotary engine of the cell. *Nature reviews Molecular cell biology* **2001**, *2*, 669–677.
- (12) Hicks, D. B.; Liu, J.; Fujisawa, M.; Krulwich, T. A. F1F0-ATP synthases of alkaliphilic bacteria: lessons from their adaptations. *Biochimica et Biophysica Acta (BBA)-Bioenergetics* **2010**, *1797*, 1362–1377.
- (13) Soga, N.; Kimura, K.; Kinosita, K.; Yoshida, M.; Suzuki, T. Perfect chemomechanical coupling of FoF1-ATP synthase. *Proceedings of the National Academy of Sciences* **2017**, *114*, 4960–4965.
- (14) Toyabe, S.; Muneyuki, E. Single molecule thermodynamics of ATP synthesis by F1-ATPase. *New Journal of Physics* **2015**, *17*, 015008.
- (15) Martin, J. L.; Ishmukhametov, R.; Spetzler, D.; Hornung, T.; Frasch, W. D. Elastic coupling power stroke mechanism of the F1-ATPase molecular motor. *Proceedings of the National Academy of Sciences* **2018**, *115*, 5750–5755.
- (16) Yanagisawa, S.; Frasch, W. D. pH-dependent 11° F₁F_o ATP synthase substeps reveal insight into the F_o torque generating mechanism. *eLife* **2021**, *10*, e70016.
- (17) Huxley, A. F.; Simmons, R. M.; Kinosita, K.; Yasuda, R.; Noji, H.; Adachi, K. A rotary molecular motor that can work at near 100% efficiency. *Philosophical Transactions of the Royal Society of London. Series B: Biological Sciences* **2000**, *355*, 473–489.

- (18) Rondelez, Y.; Tresset, G.; Nakashima, T.; Kato-Yamada, Y.; Fujita, H.; Takeuchi, S.; Noji, H. Highly coupled ATP synthesis by F₁-ATPase single molecules. *Nature* **2005**, *433*, 773–777.
- (19) Itoh, H.; Takahashi, A.; Adachi, K.; Noji, H.; Yasuda, R.; Yoshida, M.; Kinoshita, K. Mechanically driven ATP synthesis by F₁-ATPase. *Nature* **2004**, *427*, 465–468.
- (20) Noji, H.; Yasuda, R.; Yoshida, M.; Kinoshita, K. Direct observation of the rotation of F₁-ATPase. *Nature* **1997**, *386*, 299–302.
- (21) Yasuda, R.; Noji, H.; Yoshida, M.; Kinoshita, K.; Itoh, H. Resolution of distinct rotational substeps by submillisecond kinetic analysis of F₁-ATPase. *Nature* **2001**, *410*, 898–904.
- (22) Shimabukuro, K.; Yasuda, R.; Muneyuki, E.; Hara, K. Y.; Kinoshita, K.; Yoshida, M. Catalysis and rotation of F₁ motor: Cleavage of ATP at the catalytic site occurs in 1 ms before 40° substep rotation. *Proceedings of the National Academy of Sciences* **2003**, *100*, 14731–14736.
- (23) Sivak, D. A.; Crooks, G. E. Thermodynamic Metrics and Optimal Paths. *Phys. Rev. Lett.* **2012**, *108*, 190602.
- (24) Tafoya, S.; Large, S. J.; Liu, S.; Bustamante, C.; Sivak, D. A. Using a system's equilibrium behavior to reduce its energy dissipation in nonequilibrium processes. *Proceedings of the National Academy of Sciences* **2019**, *116*, 5920–5924.
- (25) Sivak, D. A.; Crooks, G. E. Thermodynamic geometry of minimum-dissipation driven barrier crossing. *Phys. Rev. E* **2016**, *94*, 052106.
- (26) Blaber, S.; Sivak, D. A. Efficient two-dimensional control of barrier crossing. *Europhysics Letters* **2022**, *139*, 17001.
- (27) Lucero, J. N. E.; Mehdizadeh, A.; Sivak, D. A. Optimal control of rotary motors. *Phys. Rev. E* **2019**, *99*, 012119.
- (28) Rotskoff, G. M.; Crooks, G. E. Optimal control in nonequilibrium systems: Dynamic Riemannian geometry of the Ising model. *Phys. Rev. E* **2015**, *92*, 060102.
- (29) Rotskoff, G. M.; Crooks, G. E.; VandenEijnden, E. Geometric approach to optimal nonequilibrium control: Minimizing dissipation in nanomagnetic spin systems. *Phys. Rev. E* **2017**, *95*, 012148.
- (30) Louwerse, M. D.; Sivak, D. A. Multi-dimensional minimum-work control of a 2D Ising model. *The Journal of Chemical Physics* **2022**, *156*, 194108.
- (31) Zulkowski, P. R.; Sivak, D. A.; Crooks, G. E.; DeWeese, M. R. Geometry of thermodynamic control. *Phys. Rev. E* **2012**, *86*, 041148.
- (32) Zulkowski, P. R.; Sivak, D. A.; DeWeese, M. R. Optimal Control of Transitions between Nonequilibrium Steady States. *PLOS ONE* **2013**, *8*, 1–7.
- (33) Zulkowski, P. R.; DeWeese, M. R. Optimal finite-time erasure of a classical bit. *Phys. Rev. E* **2014**, *89*, 052140.
- (34) Bonança, M. V. S.; Deffner, S. Optimal driving of isothermal processes close to equilibrium. *The Journal of Chemical Physics* **2014**, *140*, 244119.
- (35) Kawaguchi, K.; Sasa, S.-i.; Sagawa, T. Nonequilibrium dissipation-free transport in F₁-ATPase and the thermodynamic role of asymmetric allostereism. *Biophysical journal* **2014**, *106*, 2450–2457.
- (36) Toyabe, S.; Ueno, H.; Muneyuki, E. Recovery of state-specific potential of molecular motor from single-molecule trajectory. *EPL (Europhysics Letters)* **2012**, *97*, 40004.

- (37) Toyabe, S.; Watanabe-Nakayama, T.; Okamoto, T.; Kudo, S.; Muneyuki, E. Thermodynamic efficiency and mechanochemical coupling of F1-ATPase. *Proceedings of the National Academy of Sciences* **2011**, *108*, 17951–17956.
- (38) See Supplemental Material at [URL will be inserted by publisher] for more numerical simulation results.
- (39) Saita, E.-i.; Suzuki, T.; Kinoshita, K.; Yoshida, M. Simple mechanism whereby the F1-ATPase motor rotates with near-perfect chemomechanical energy conversion. *Proc. Nat. Acad. Sci.* **2015**, *112*, 9626–9631.
- (40) Palanisami, A.; Okamoto, T. Torque-Induced Slip of the Rotary Motor F1-ATPase. *Nano Lett.* **2010**, *10*, 4146–4149.
- (41) Risken, H.; Frank, T. *The Fokker-Planck Equation: Methods of Solution and Applications*; Springer Series in Synergetics; Springer Berlin Heidelberg, 1996.
- (42) Nakazato, M.; Ito, S. Geometrical aspects of entropy production in stochastic thermodynamics based on Wasserstein distance. *Phys. Rev. Research* **2021**, *3*, 043093.
- (43) Ito, S. Geometric thermodynamics for the Fokker-Planck equation: Stochastic thermodynamic links between information geometry and optimal transport. 2022; <https://arxiv.org/abs/2209.00527>.
- (44) Schmiedl, T.; Seifert, U. Optimal Finite-Time Processes In Stochastic Thermodynamics. *Phys. Rev. Lett.* **2007**, *98*, 108301.
- (45) Gomez-Marin, A.; Schmiedl, T.; Seifert, U. Optimal protocols for minimal work processes in underdamped stochastic thermodynamics. *The Journal of Chemical Physics* **2008**, *129*, 024114.
- (46) Blaber, S.; Louwerse, M. D.; Sivak, D. A. Steps minimize dissipation in rapidly driven stochastic systems. *Phys. Rev. E* **2021**, *104*, L022101.
- (47) Engel, M. C.; Smith, J. A.; Brenner, M. P. Optimal control of nonequilibrium systems through automatic differentiation. 2022; <https://arxiv.org/abs/2201.00098>.
- (48) Zhong, A.; DeWeese, M. R. Limited-control optimal protocols arbitrarily far from equilibrium. *Phys. Rev. E* **2022**, *106*, 044135.
- (49) Gingrich, T. R.; Rotskoff, G. M.; Crooks, G. E.; Geissler, P. L. Near-optimal protocols in complex nonequilibrium transformations. *Proceedings of the National Academy of Sciences* **2016**, *113*, 10263–10268.
- (50) Silverstein, T. P. An exploration of how the thermodynamic efficiency of bioenergetic membrane systems varies with c-subunit stoichiometry of F₁ F_o ATP synthases. *Journal of bioenergetics and biomembranes* **2014**, *46*, 229–241.
- (51) Plischke, M.; Bergersen, B. *Equilibrium Statistical Physics*; World Scientific, 2006.
- (52) Ref. 25, App. B.